HYPERSONIC FLOW OVER AN ELLIPTIC CONE: THEORY AND EXPERIMENT

Thesis by

Robert L. Chapkis

In Partial Fulfillment of the Requirements

For the Degree of

Aeronautical Engineer

California Institute of Technology

Pasadena, California

1959

ACKNOWLEDGMENTS

The author expresses deep appreciation to Professor Lester Lees for his guidance, help, and encouragement throughout this investigation. He also thanks the staff of the hypersonic group for their help and advice during the course of the experiment; the Aeronautics machine shop for constructing the model and various other pieces of equipment; Mrs. Betty Laue for carefully performing the computations and preparing the graphs; Mrs. Geraldine Van Gieson for typing the manuscript; and Mrs. Betty Wood for inking the equations.

ABSTRACT

By applying hypersonic approximations to Ferri's linearized characteristics method simple results were obtained for the shock shape and surface pressure distribution for an unyawed conical body of arbitrary cross-section. Calculations were carried out for an elliptic cone having a ratio of major to minor axis of 2:1, and a semi-vertex angle of about 12° in the meridian plane containing the major axis. An experimental investigation of the flow over this body conducted at a Mach number of 5.8 in the GALCIT hypersonic wind tunnel showed that the surface pressure distribution at zero angle of attack agreed quite closely with the theoretical prediction. On the other hand the simple Newtonian approximation predicts pressures that are too low.

Surface pressure distributions and schlieren photographs of the shock shape were also obtained at angles of attack up to 14° at zero yaw, and at angles of yaw up to 10°, at zero pitch. At the higher angles of attack the Newtonian approximation for the surface pressures is quite accurate.

TABLE OF CONTENTS

LIST OF FIGURES

LIST OF SYMBOLS

a	speed of sound, referred to limiting velocity
C_p	pressure coefficient
M_1	free stream Mach number
R	gas constant
s	entropy
u, v, w	velocity components in spherical coordinates, referred to limiting velocity (See Figure 1.)
V	local resultant velocity, referred to limiting velocity
V_1	undisturbed velocity, referred to limiting velocity
$r, \theta,$	spherical coordinates (See Figure 1.)
α	angle of attack
γ	ratio of specific heats
ψ	angle of yaw

Subscripts

n, m	index of summation
o	properties of the basic axially symmetric conical flow
c	properties at the body surface
s	properties at the shock wave

I. INTRODUCTION

Studies of the flow past elliptic cones are of interest for two reasons: (1) As Van Dyke has pointed out[1], the elliptic cone will probably become a standard of comparison for supersonic flow past bodies without axial symmetry, just as the circular cone is used as a standard of comparison for supersonic flow past bodies of revolution; (2) Elliptic cones may have important aerodynamic advantages over circular cones. For example, both theoretical and experimental investigations[2-5] have shown that an elliptic cone may have significantly higher lift-drag ratios than a circular cone of the same cross sectional area per unit length.

Most of the theoretical investigations of the flow about elliptic cones are based upon linearizing assumptions which are not valid at very high Mach numbers. Even Van Dyke's second-order theory[1], which proceeds from slender body theory and includes the effect of the leading non-linear terms in the equations of motion, cannot be expected to give good results in the hypersonic speed range.

At hypersonic speeds the well-known Newtonian approximation (or a suitable modification)[3] has been quite successful in predicting surface pressure distributions, provided that the component of Mach number normal to the surface is of order unity, or larger. But for "flat" bodies, such as a delta wing or an elliptic cone of significant eccentricity, this restriction means that the free stream Mach number must be extremely high, or the angle of pitch (or yaw) must be large. For example, the Newtonian approximation states that the shock wave

coincides with the body surface, at least to first order. However, on physical grounds the cross-section of the shock surface for an unyawed elliptic cone is expected to have a smaller eccentricity than the body cross-section, except possibly in the limiting case $(\gamma - 1) M_\infty^2 \longrightarrow \infty$. This fact must have a significant effect on the surface pressure distribution.

In view of these criticisms, it seems desirable to work out a solution for the unyawed elliptic cone at hypersonic speeds directly from the gasdynamic equations of motion. One attractive approach to this problem is the "linearized characteristics method" developed by Ferri and co-workers[2,6], which considers the flow about a body to be a perturbation of a known basic non-linear flow field. Thus the flow about an elliptic cone is considered as being a perturbation of the known flow field about a circular cone. Only linear terms in the perturbation quantities are retained in the differential equations and boundary conditions. It should be noted that the linearization is with respect to deviations from a known basic flow field which is "close" to the actual flow field, and not with respect to deviations from the uniform flow upstream of the shock wave. This method should be applicable for hypersonic as well as supersonic flows, provided that the "exact" basic flow field is known.

Ness and Kaplita[7] utilized Ferri's scheme and the results of Kopal's computations for the unyawed circular cone to calculate the perturbation velocities for any body which employs the circular cone flow field as a basic flow. Their calculation entails a step-by-step numerical integration of the governing differential equations for each particular case. Now for hypersonic flow this difficulty can be

circumvented by employing the hypersonic approximation for the flow over a circular cone obtained by Lees[8]. By expanding the velocity components in a Taylor's series in the conical ray angle, Lees obtained simple approximate expressions for the velocity components, shock wave angle, and pressure coefficient. These approximate expressions give results which agree very well with the actual values computed by Kopal, provided that the hypersonic similarity parameter $K = M_1 \theta_{oc}$ is greater than about one. By substituting these approximate expressions for the circular-cone velocity components into the differential equation governing the perturbation velocities for a body of non-circular cross-section, this equation is greatly simplified. In fact simple algebraic expressions are obtained for these perturbation velocities (Part II). Once these quantities are known the surface pressure distribution and the Fourier coefficients for the shock shape are readily calculated.

The ultimate test of the theoretical analysis must be made by comparing it with an "exact" solution or with experimental results. Several experimental investigations have been made of the flow over elliptic cones at low and moderate supersonic Mach numbers (up to about Mach 3)[5, 9, 10]. However, no experimental results were available at hypersonic speeds. Therefore, an experimental investigation of the flow over an elliptic cone was carried out in the GALCIT M = 5.8 wind tunnel, in order to obtain surface pressure distributions and shock wave shapes at zero angle of attack and also at various angles of attack and of yaw. The description and results of the experimental investigation are presented in Part III.

II. THEORETICAL INVESTIGATION

A. Resume of Linearized Characteristics Method

By combining the continuity, momentum, and energy equations for a non-viscous perfect gas, the following equations are obtained for the case of conical flow:

$$u\left(2 - \frac{v^2 + w^2}{a^2}\right) + v \cot\theta + \frac{\partial v}{\partial \theta}\left(1 - \frac{v^2}{a^2}\right) + \frac{1}{\sin\theta}\frac{\partial w}{\partial \phi}\left(1 - \frac{w^2}{a^2}\right) - \frac{wv}{a^2}\left(\frac{1}{\sin\theta}\frac{\partial v}{\partial \phi} + \frac{\partial w}{\partial \theta}\right) = 0 \tag{1}$$

$$\frac{a^2}{\gamma R}\frac{\partial s}{\partial \phi} = v \sin\theta \frac{\partial w}{\partial \theta} - u\frac{\partial u}{\partial \phi} - v\frac{\partial v}{\partial \phi} + w\,u \sin\theta + w\,v\cos\theta \tag{2}$$

$$\frac{a^2}{\gamma R}\frac{\partial s}{\partial \theta} = -u\frac{\partial u}{\partial \theta} - w\frac{\partial w}{\partial \theta} + \frac{w}{\sin\theta}\frac{\partial v}{\partial \phi} + u\,v - w^2\cot\theta \tag{3}$$

where the directions of u, v, w, θ, and ϕ are shown in Figure 1.

Immediately downstream of the shock front, i. e., at $\theta = \theta_s$, the following relations exist:

$$(u)_{\theta_s} = V_1 \cos\theta_s \tag{4}$$

$$(v)_{\theta_s} = -\frac{\gamma - 1}{\gamma + 1}\left(\frac{1 - V_1^2\cos^2\theta_s - V_1^2\sin^2\theta_s\sin^2\beta}{V_1\sin\theta_s}\right) - V_1\sin\theta_s\sin^2\beta \tag{5}$$

$$(w)_{\theta_s} = -V_1\sin\theta_s\sin\beta\cos\beta + \frac{\gamma - 1}{\gamma + 1}\left(1 - V_1^2\cos^2\theta_s - V_1^2\sin^2\theta_s\sin^2\beta\right)\frac{\tan\beta}{V_1\sin\theta_s} \tag{6}$$

where θ_s is the shock wave angle, and β is defined by

$$\tan \beta = \frac{1}{\sin \theta_s} \frac{d\theta_s}{d\phi} \tag{7}$$

The shock wave angle θ_s is expanded in a Fourier series:

$$\theta_s = \theta_{os} + \sum \theta_{ns} \cos n\phi + \sum \theta_{ms} \sin m\phi , \tag{8}$$

where θ_{os} is the shock angle for the basic circular cone. In Ferri's analysis only first order terms in θ_{ns} and θ_{ms} are retained in the differential equations and boundary conditions. To this approximation, series representations of the velocity components which are consistent with the conditions just behind the shock front are as follows:

$$u = u_o + \sum \theta_{ns} u_n \cos n\phi + \sum \theta_{ms} u_m \sin m\phi \tag{9}$$

$$v = v_o + \sum \theta_{ns} v_n \cos n\phi + \sum \theta_{ms} v_m \sin m\phi \tag{10}$$

$$w = \sum n \theta_{ns} w_n \sin n\phi + \sum m \theta_{ms} w_m \cos m\phi \tag{11}$$

where u_n, u_m, etc. are functions of θ.

By expanding u, v, and w in a Taylor's series around $\theta = \theta_{os}$, and recognizing that $\theta_s = \theta_{os} + (\theta_s - \theta_{os})$, the shock conditions [Equations (4) - (6)] can be made to yield the following relations for u_n, u_m, etc. at $\theta = \theta_{os}$, independently of n and m:

$$(u_n)_{\theta_{os}} = (u_m)_{\theta_{os}} = - V_1 \sin \theta_{os} (v_o)_{\theta_{os}} \tag{12}$$

$$(v_n)_{\theta_{os}} = (v_m)_{\theta_{os}} = - \frac{\gamma - 1}{\gamma + 1} \cos \theta_{os} \left(2V_1 - \frac{1 - V_1^2 \cos^2 \theta_{os}}{V_1 \sin^2 \theta_{os}}\right) + \left(\frac{\partial v_o}{\partial \theta}\right)_{\theta_{os}} \tag{13}$$

$$(w_n)_{\theta_{os}} = (w_m)_{\theta_{os}} = V_1 + \frac{1}{\sin \theta_{os}} (v_o)_{\theta_{os}} \tag{14}$$

Here u_o and v_o are the radial and normal velocity components corresponding to the flow about a circular cone of semi-vertex angle θ_{oc}. The shock wave angle for the flow about the circular cone is θ_{os}. At $\theta = \theta_{os}$:

$$(u_o)_{\theta_{os}} = V_1 \cos \theta_{os} \tag{15}$$

$$(v_o)_{\theta_{os}} = - \frac{\gamma - 1}{\gamma + 1} \left(\frac{1 - V_1^2 \cos^2 \theta_{os}}{V_1 \sin \theta_{os}} \right) \tag{16}$$

$$\left(\frac{\partial v_o}{\partial \theta} \right)_{\theta_{os}} = - \left[u_o + \frac{u_o + v_o \cot \theta_{os}}{1 - (v_o/a_o)^2} \right]_{\theta_{os}} \tag{17}$$

When the series for u, v, and w are substituted into Equation (1) and only first-order terms in θ_{ns} and θ_{ms} are retained, three independent equations result. As expected the quantities u_o and v_o satisfy the differential equation governing axially symmetric conical flow:

$$u_o \left[2 - \left(\frac{v_o}{a_o} \right)^2 \right] + v_o \cot \theta + \frac{\partial v_o}{\partial \theta} \left[1 - \left(\frac{v_o}{a_o} \right)^2 \right] = 0 \tag{18}$$

The second equation is

$$\begin{aligned} &\frac{\partial v_n}{\partial \theta} + v_n \cot \theta + 2 u_n + \frac{n^2 w_n}{\sin \theta} \\ &= \left(\frac{v_o}{a_o} \right)^2 \frac{\partial v_n}{\partial \theta} - \left[\frac{\left(\frac{v_o}{a_o} \right)\left(\frac{u_o}{a_o} \right) + \left(\frac{v_o}{a_o} \right)^2 \cot \theta}{1 - \left(\frac{v_o}{a_o} \right)^2} \right] \left[2 + (\gamma - 1) \left(\frac{v_o}{a_o} \right)^2 \right] v_n \\ &+ \left\{ \left(\frac{v_o}{a_o} \right)^2 - \left[\frac{\left(\frac{v_o}{a_o} \right)\left(\frac{u_o}{a_o} \right) + \left(\frac{v_o}{a_o} \right)^2 \cot \theta}{1 - (v_o/a_o)^2} \right] (\gamma - 1) \left(\frac{u_o}{a_o} \right)\left(\frac{v_o}{a_o} \right) \right\} u_n \end{aligned} \tag{19}$$

The third equation is exactly the same as Equation (19) but with the subscript n replaced by m.

In order to solve for u_n, v_n, and w_m, two more relations between u_n, v_n, and w_n are needed in addition to Equation (19). Ferri obtains these relations from Equations (2) and (3) and the momentum equation in the radial direction. To the first approximation in θ_n and θ_m :

$$v_n = \frac{\partial u_n}{\partial \theta} \quad , \quad v_o = \frac{\partial u_o}{\partial \theta} \tag{20}$$

and

$$-\frac{a_o^2}{\gamma R} s' = v_o \sin\theta \frac{\partial w}{\partial \theta} + u_o u_n + v_o v_n + u_o w_n \sin\theta + v_o w_n \cos\theta \tag{21}$$

where $s' = \left(\frac{ds}{d\theta_s}\right)_{\theta_{os}}$ is the rate of change of entropy with respect to shock angle. By utilizing Equation (20), Equation (21) can be written as

$$-\frac{a_o^2}{\gamma R} s' = u_o (u_n + w_n \sin\theta) + v_o \frac{\partial}{\partial \theta}(u_n + w_n \sin\theta) \tag{22}$$

or,

$$u_n + w_n \sin\theta = -\left(\frac{s'}{\gamma R}\right) a_o^{1/\gamma - 1} (-v_o \sin\theta)^{\frac{1}{2}} \int_{\theta_{os}}^{\theta} \frac{a_o^{(2-3)/-1}}{v_o (-v_o \sin\theta)^{1/2}} d\theta \tag{23}$$

The relations between u_m, v_m, and w_m are the same as Equations (20) and (23), with the subscript n replaced by m. Equations (19), (20), and (23) plus a knowledge of the values of u_o, v_o, and θ_{os} enable u_n, u_m, etc. to be computed numerically.

The boundary conditions at the surface of the body enable one to determine the shock coefficients, θ_{ms} and θ_{ns}, once v_n and v_m are determined. The boundary condition at the surface of the body is that the velocity component normal to the surface of the body be zero, or for conical bodies:

$$\left(\frac{v}{w}\right)_{\theta_c} = \frac{1}{\sin\theta_c}\,\frac{d\theta_c}{d\phi} \tag{24}$$

The shape of the body as defined by $\theta_c = \theta_c(\phi)$ is now also expressed in a Fourier series as follows:

$$\theta_c = \theta_{oc} + \sum \theta_{nc} \cos n\phi + \sum \theta_{mc} \sin m\phi \tag{25}$$

One observes that $\left(\frac{v}{w}\right)_{\theta_{oc}}$ is of order θ_{nc}, and w is of order θ_{ns}, so that v is of order $\theta_{ns}\ \theta_{nc}$; i.e., $(v)_{\theta_c} = 0$ to first order. Now v and w are expanded in a Taylor's series about $\theta = \theta_{oc}$. If only first order terms in θ_{nc}, θ_{mc}, θ_{ns}, and θ_{ms} are retained then:

$$(v)_{\theta_c} = (v_o)_{\theta_{oc}} + \left(\frac{\partial v_o}{\partial\theta}\right)_{\theta_{oc}} (\theta_c - \theta_{oc}) + \sum \theta_{ns} (v_n)_{\theta_{oc}} \cos n\phi + \sum \theta_{ms} (v_m)_{\theta_{oc}} \sin m\phi \tag{27}$$

and

$$(w)_{\theta_c} = \sum \theta_{ns} (w_n)_{\theta_{oc}}\, n \sin n\phi + \sum \theta_{ms} (w_m)_{\theta_{oc}}\, m \cos m\phi \tag{28}$$

and since $(v)_{\theta_c} = 0$, then:

$$(v_o)_{\theta_{oc}} + \left(\frac{\partial v_o}{\partial\theta}\right)_{\theta_{oc}} \left(\sum \theta_{nc} \cos n\phi + \sum \theta_{mc} \sin m\phi\right) = -\sum \theta_{ns} (v_n)_{\theta_{oc}} \cos n\phi - \sum \theta_{ms} (v_m)_{\theta_{oc}} \sin m\phi \tag{29}$$

But $(v_o)_{\theta_{oc}} = 0$, and $\left(\frac{\partial v_o}{\partial \theta}\right)_{\theta_{oc}} = -2\,(u_o)_{\theta_{oc}}$, therefore,

$$\theta_{ns} = 2\,\theta_{nc}\left(\frac{u_o}{v_n}\right)_{\theta_{oc}}$$

$$\theta_{ms} = 2\,\theta_{mc}\left(\frac{u_o}{v_m}\right)_{\theta_{oc}} \tag{34}$$

The pressure distribution is obtained from the expression

$$C_p = \frac{2}{\gamma M_1^2}\left[\left(\frac{1 - V^2}{1 - V_1^2}\right)^{\gamma/\gamma-1} e^{-\Delta s/R} - 1\right] \tag{35}$$

The square of the magnitude of the velocity on the surface of the body is

$$V^2 = \left[(u_o)_{\theta_{oc}} + \sum \theta_{ns}\,(u_n)_{\theta_{oc}} \cos n\phi + \sum \theta_{ms}\,(u_m)_{\theta_{oc}} \sin m\phi\right]^2$$

$$+\left[\sum n\,\theta_{ns}\,(w_n)_{\theta_{oc}} \sin n\phi + \sum m\,\theta_{ms}\,(w_m)_{\theta_{oc}} \cos m\phi\right]^2 \tag{36}$$

since to the approximation accepted, $(v)_{\theta_c} = 0$. Ferri shows that $\frac{\partial s}{\partial \theta}$ is of order $(\theta_{ns})^2$; therefore, the entropy behind the shock front is taken as constant in any meridian plane. Thus Δ s is equal to its value across the shock wave.

B. Hypersonic Approximation

In this section, approximations valid for hypersonic flow are applied to Equations (19) and (23) which will enable simple algebraic expressions to be obtained for u_n, v_n, and w_n.

First of all Equation (19) will be written in a more convenient form. Solving for $\partial v_o/\partial\theta$ from Equation (18), it is easily seen that

$$-\frac{v_o}{a_o^2}\left(u_o + \frac{\partial v_o}{\partial\theta}\right) = \frac{\left(\frac{v_o}{a_o}\right)\left(\frac{u_o}{a_o}\right) + \left(\frac{v_o}{a_o}\right)^2 \cot\theta}{1 - \left(\frac{v_o}{a_o}\right)^2}$$

Therefore Equation (19) can be written in the form

$$\frac{\partial v_n}{\partial\theta} + v_n \cot\theta + 2u_n + \frac{n^2 w_n}{\sin\theta}$$

$$= \left(\frac{v_o}{a_o}\right)^2 \frac{\partial v_n}{\partial\theta} + \frac{v_o}{a_o^2}\left(u_o + \frac{\partial v_o}{\partial\theta}\right)\left[2 + (\gamma - 1)\left(\frac{v_o}{a_o}\right)^2\right] v_n \qquad (37)$$

$$+ \left[\left(\frac{v_o}{a_o}\right)^2 + \frac{v_o}{a_o^2}\left(u_o + \frac{\partial v_o}{\partial\theta}\right)(\gamma - 1)\left(\frac{u_o}{a_o}\right)\left(\frac{v_o}{a_o}\right)\right] u_n$$

The coefficients of u_n, v_n, and $\frac{\partial v_n}{\partial\theta}$ on the right-hand side of Equation (37) involve only the axisymmetrical conical flow. This equation can be greatly simplified for the case of hypersonic flow by making use of the series representations for u_o and v_o which were derived by Lees in Reference 8. The series are the following:

$$u_o = (u_o)_{\theta_{oc}} \left[1 - (\theta - \theta_{oc})^2 + \frac{1}{3} \cot \theta_{oc} (\theta - \theta_{oc})^3 - a_4 (\theta - \theta_{oc})^4 + \ldots \right]$$

$$v_o = (u_o)_{\theta_{oc}} \left[-2 (\theta - \theta_{oc}) + \cot \theta_{oc} (\theta - \theta_{oc})^2 - 4a_4 (\theta - \theta_{oc})^3 \ldots \right] \quad (38)$$

where

$$a_4 = \frac{1}{4} \cot^2 \theta_{oc} + \frac{2}{3(\gamma - 1)} \left(\frac{u_o^2}{1 - u_o^2} \right)_{\theta_{oc}}$$

In this analysis it is assumed that $(\theta - \theta_{oc}) \cot \theta_{oc}$ is much less than one, which implies that the shock wave is "close" to the body surface. If this assumption is made throughout the analysis, and if Equations (38) are substituted into Equation (37), the following equation is obtained:

$$\frac{\partial v_n}{\partial \theta} + v_n \cot \theta + 2 u_n + \frac{n^2 w_n}{\sin \theta}$$

$$= \frac{8}{\gamma - 1} \left(\frac{u_o^2}{1 - u_o^2} \right)_{\theta_{oc}} \left[(\theta - \theta_{oc})^2 \frac{\partial v_n}{\partial \theta} + (\theta - \theta_{oc}) v_n \right. \quad (39)$$

$$\left. + 2 \left(\frac{u_o^2}{1 - u_o^2} \right)_{\theta_{oc}} (\theta - \theta_{oc})^2 u_n \right]$$

However, $$\left(\frac{u_o^2}{1 - u_o^2} \right)_{\theta_{oc}} \cong \frac{1}{2} \frac{\gamma - 1}{\gamma + 1} \frac{\cot \theta_{os}}{\theta_{os} - \theta_{oc}} \quad * \quad (40)$$

Thus Equation (39) reduces to the following:

$$\frac{\partial v_n}{\partial \theta} + v_n \cot \theta + 2 u_n + \frac{n^2 w_n}{\sin \theta} \cong \frac{4}{\gamma + 1} \left(\frac{\theta - \theta_{oc}}{\theta_{os} - \theta_{oc}} \right) v_n \cot \theta_{os} \quad (41)$$

---

* This relation is derived in Appendix 1.

In a similar manner, Equation (23) relating u_n and w_n is simplified by utilizing the series for u_o and v_o valid for hypersonic flow. If in addition, one makes the slender-body hypersonic approximation, then $\cot\theta \cong \frac{1}{\sin\theta} \cong \frac{1}{\theta}$, and Equation (23) reduces to the following form:

$$u_n + w_n \sin\theta = -\frac{\gamma-1}{2}\left(\frac{1-u_o^2}{u_o}\right)_{\theta_{oc}}\left(\frac{s'}{\gamma R}\right)\left(\frac{\theta}{\theta_{oc}}\right)\left[1-\left(\frac{\theta_{oc}}{\theta}\right)^{\frac{1}{2}}\left(\frac{\theta-\theta_{oc}}{\theta_{os}-\theta_{oc}}\right)^{\frac{1}{2}}\right] \tag{42}$$

Now Equations (20) and (42) are used to write Equation (41) in terms of u_n only:

$$\frac{\partial^2 u_n}{\partial\theta^2} + \frac{1}{\theta}\frac{\partial u_n}{\partial\theta} + \left(2-\frac{n^2}{\theta^2}\right)u_n = \frac{4}{\gamma+1}\left(\frac{\theta-\theta_{oc}}{\theta_{os}-\theta_{oc}}\right)\frac{1}{\theta_{os}}\frac{\partial u_n}{\partial\theta}$$
$$-\frac{n^2}{\theta^2}\left[\frac{\gamma-1}{2}\left(\frac{1-u_o^2}{u_o}\right)_{\theta_{oc}}\frac{s'}{\gamma R}\left(\frac{\theta}{\theta_{oc}}\right)\right]\left[1-\left(\frac{\theta_{os}}{\theta}\right)^{\frac{1}{2}}\left(\frac{\theta-\theta_{oc}}{\theta_{os}-\theta_{oc}}\right)^{\frac{1}{2}}\right] \tag{43}$$

Now it turns out that the second term on the right-hand side involving $ds/d\theta_s$ makes only a small contribution to the solution for u_n, and the contribution of the first term involving $\partial u_n/\partial\theta$ is even smaller. Therefore, a first approximation for u_n is obtained by neglecting the first term on the right hand side of Equation (43). Also, it is assumed that n^2/θ^2 is much larger than 2, which is certainly true for a slender body. If these assumptions are made, then the solution of the homogeneous equation for u_n is as follows:

$$
\left.
\begin{aligned}
(u_n)_{\text{homogeneous}} &= A\theta^n + B\theta^{-n} \\
(v_n)_{\text{homogeneous}} &= \frac{\partial u_n}{\partial \theta} = \frac{n}{\theta}\left(A\theta^n - B\theta^{-n}\right) \\
\text{where} \qquad A &= \tfrac{1}{2}\,\theta_{os}^{-n}\left[(u_n)_{\theta_{os}} + \frac{\theta_{os}}{n}(v_n)_{\theta_{os}}\right] \\
B &= \tfrac{1}{2}\,\theta_{os}^{\,n}\left[(u_n)_{\theta_{os}} - \frac{\theta_{os}}{n}(v_n)_{\theta_{os}}\right]
\end{aligned}
\right\} \qquad (44)
$$

Thus

$$
\begin{aligned}
(u_n)_{\text{homogeneous}} &= -\frac{\theta_{os}}{2n}(v_n)_{\theta_{os}}\left[\left(\frac{\theta_{os}}{\theta}\right)^n - \left(\frac{\theta}{\theta_{os}}\right)^n\right] \\
&\quad + \tfrac{1}{2}(u_n)_{\theta_{os}}\left[\left(\frac{\theta_{os}}{\theta}\right)^n + \left(\frac{\theta}{\theta_{os}}\right)^n\right] \\
&= -\frac{\theta}{n}\left\{\tfrac{1}{2}(v_n)_{\theta_{os}}\left[\left(\frac{\theta_{os}}{\theta}\right)^{n+1} - \left(\frac{\theta}{\theta_{os}}\right)^{n-1}\right]\right. \\
&\quad \left. - \frac{n}{2}(u_n)_{\theta_{os}}\left(\frac{\theta_{os}}{\theta^2}\right)\left[\left(\frac{\theta_{os}}{\theta}\right)^{n-1} + \left(\frac{\theta}{\theta_{os}}\right)^{n+1}\right]\right\} \qquad (45)
\end{aligned}
$$

$$
\begin{aligned}
(v_n)_{\text{homogeneous}} &= \tfrac{1}{2}(v_n)_{\theta_{os}}\left[\left(\frac{\theta_{os}}{\theta}\right)^{n+1} + \left(\frac{\theta}{\theta_{os}}\right)^{n-1}\right] \\
&\quad - \frac{n}{2}(u_n)_{\theta_{os}}\left(\frac{\theta_{os}}{\theta^2}\right)\left[\left(\frac{\theta_{os}}{\theta}\right)^{n-1} - \left(\frac{\theta}{\theta_{os}}\right)^{n+1}\right]
\end{aligned}
$$

The particular solution for u_n can be obtained by the method of variation of parameters, as follows:

$$(u_n)_{particular} = \frac{\gamma+1}{2}\left(\frac{1-u_o^2}{u_o}\right)_{\theta_{oc}} \frac{s'}{\gamma R}\frac{n}{2\theta_{oc}}\int_{\theta_{os}}^{\theta}\left[\left(\frac{\theta}{t}\right)^n-\left(\frac{t}{\theta}\right)^n\right] \times\left[1-\left(\frac{\theta_{os}}{t}\right)^{\frac{1}{2}}\left(\frac{t-\theta_{oc}}{\theta_{os}-\theta_{oc}}\right)^{\frac{1}{2}}\right] dt \tag{46}$$

A correction to the first approximation for u_n is derived by substituting the expression for $\partial u_n/\partial\theta$ from Equation (44) into the first term on the right hand side of Equation (43). The method of variation of parameters is then used to obtain a particular solution which is a correction to the first approximation for u_n. This procedure is carried out in Appendix 2.

According to Equations (12), (13), (15), and (16) the values of $(u_n)_{\theta_{os}}$ and $(v_n)_{\theta_{os}}$ depend only on the axisymmetrical conical flow, as follows:

$$(u_n)_{\theta_{os}} = -(u_o)_{\theta_{os}} \tan\theta_{os} - (v_o)_{\theta_{os}} \tag{47}$$

$$(v_n)_{\theta_{os}} = -2\frac{\gamma+1}{\gamma+1}(u_o)_{\theta_{os}} - (v_o)_{\theta_{os}}\cot\theta_{os} - \left(\frac{\partial v_o}{\partial\theta}\right)_{\theta_{os}} \tag{48}$$

By utilizing Equations (17) and (39), one finds that

$$\left(\frac{\partial v_o}{\partial\theta}\right)_{\theta_{os}} = -\left[u_o - \frac{2}{\gamma+1}\frac{a_o^2}{v_o}\cot\theta\right]_{\theta_{os}}$$

$$= -2(u_o)_{\theta_{os}} - \frac{\gamma+1}{\gamma+1}(v_o)_{\theta_{os}}\cot\theta_{os}$$

Therefore, $(v_n)_{\theta_{os}}$ can be written in the following form:

$$(v_n)_{\theta_{os}} = \frac{2}{\gamma+1}\left[2\,(u_o)_{\theta_{os}} - (v_o)_{\theta_{os}}\cot\theta_{os}\right] \tag{49}$$

By substituting the series for u_o anv v_o into Equations (47) and (49), approximate expressions for $(u_n)_{\theta_{os}}$ and $(v_n)_{\theta_{os}}$ are now obtained:

$$\begin{aligned}(u_n)_{\theta_{os}} &\cong -(u_o)_{\theta_{oc}}\,\theta_{os}\left(\frac{\theta_{oc}}{\theta_{os}}\right)^2 \\ (v_n)_{\theta_{os}} &\cong (u_o)_{\theta_{oc}}\left[\frac{4}{\gamma+1}\left(1+\frac{\theta_{os}-\theta_{oc}}{\theta_{os}}\right)\right] \cong \frac{4}{\gamma+1}\,(u_o)_{\theta_{oc}}\end{aligned} \tag{50}$$

When these relations are employed in Equations (45), the expressions for $(u_n)_{\theta_{oc}}$ and $(v_n)_{\theta_{oc}}$ take the following form:

$$\begin{aligned}\left(\frac{u_n}{u_o}\right)_{\theta_{oc}} = -\frac{\theta_{oc}}{n}\Bigg\{&\frac{2}{\gamma+1}\left[\left(\frac{\theta_{os}}{\theta_{oc}}\right)^{n+1} - \left(\frac{\theta_{oc}}{\theta_{os}}\right)^{n-1}\right] \\ &+ \frac{n}{2}\left[\left(\frac{\theta_{os}}{\theta_{oc}}\right)^{n-1} + \left(\frac{\theta_{oc}}{\theta_{os}}\right)^{n+1}\right]\Bigg\}\end{aligned} \tag{51}$$

$$\begin{aligned}\left(\frac{v_n}{u_o}\right)_{\theta_{oc}} = &\frac{2}{\gamma+1}\left[\left(\frac{\theta_{os}}{\theta_{oc}}\right)^{n+1} + \left(\frac{\theta_{oc}}{\theta_{os}}\right)^{n-1}\right] \\ &+ \frac{n}{2}\left[\left(\frac{\theta_{os}}{\theta_{oc}}\right)^{n-1} - \left(\frac{\theta_{oc}}{\theta_{os}}\right)^{n+1}\right]\end{aligned}$$

and from Equation (42):

$$\left(\frac{w_n}{u_o}\right)_{\theta_{oc}} = -\frac{1}{\sin\theta_{oc}}\left(\frac{u_n}{u_o}\right)_{\theta_{oc}} - \frac{\gamma-1}{2}\left(\frac{1-u_o^2}{u_o^2}\right)_{\theta_{oc}}\left(\frac{s'}{\gamma R}\right) \tag{52}$$

where

$$\frac{\gamma-1}{2}\left(\frac{1-u_o^2}{u_o^2}\right)_{\theta_{oc}}\left(\frac{s'}{\gamma R}\right) \cong \frac{2}{M_1 K_s}\left[\frac{(K_s^2-1)^2}{2\gamma K_s^2-(\gamma-1)}\right]$$

and $K_s \equiv M_1 \theta_{os}$. This expression for $\frac{\gamma-1}{2}\left(\frac{1-u_o^2}{u_o^2}\right)_{\theta_{oc}}\left(\frac{s'}{\gamma R}\right)$ is derived in Appendix 1.

The expressions for u_m, v_m, and w_m are the same as those for u_n, v_n, and w_n, but with the subscript n replaced by m.

By using Equation (35) for C_p and Equations (51), (52), and (34) the surface pressure distribution is calculated. Shock shape is calculated using Equations (8) and (34).

Although the present calculation is carried out for a particular elliptic cone, evidently the procedure is applicable to a conical body of arbitrary cross-section at hypersonic speeds.

III. EXPERIMENTAL INVESTIGATION OF HYPERSONIC FLOW OVER AN ELLIPTIC CONE

A. Description of the Experiment

1. Model and Equipment

The experiment was conducted in the GALCIT 5 x 5 inch hypersonic wind tunnel, which is a closed-return, continuously operating tunnel. All of the tests were made at a fixed reservoir temperature of 250°F and a fixed stagnation pressure of 74 psi gage, giving a nominal test section Mach number of 5.8 and a Reynolds number per inch of 2.2×10^5. An extensive description of the experimental facilities is given in Reference 11.

The elliptic cone model was constructed of brass, and the length of the model from tip to base was 4-3/16". The major to minor axis ratio of the elliptic cross section was two; the major axis being 1-3/4" long at the base, and the minor axis 7/8" long.

Twelve .016" diameter pressure orifices were located around the periphery of the cone in a section 1-15/16" from the tip. The angular locations of the orifices are shown in Figure 2. Note that there are four orifices which are spaced 90° apart, two along the ends of a major axis, and two along the ends of a minor axis. These four orifices enabled the model to be aligned with the flow direction.

The surface pressures were measured by means of a multi-tube vacuum-referenced silicone oil manometer.

As shown in Figure 3, the model was mounted in the wind tunnel on a 1/2" diameter sting which was supported by two vertical struts

extending through the top of the test section. The vertical struts were individually raised or lowered by external controls to adjust the pitch angle of the model. It can be seen in Figure 3 that the rear vertical strut is not connected directly to the sting but that there is an intermediate short piece of steel. This short piece of steel could be moved from side to side by means of an attached wire passing through a hole in the side of the wind tunnel. Small corrections for yaw misalignment could be made by pushing or pulling the wire from outside of the wind tunnel.

In order to obtain angles of attack above ten degrees, it was necessary to use a sting with a ten degree bend where the sting attached to the model.

2. Test Procedure

The model was positioned on the tunnel axis and the tunnel operated for at least one hour to allow the tunnel air temperature to stabilize. The model was then adjusted by means of the external controls so that the pressures at the orifices at the ends of the minor axis read the same, and this position was taken as zero angle of attack. Also the model was adjusted so that the pressures at the orifices at the ends of the major axis read the same, so that the yaw angle was zero also. Using this position as a reference, the model was pitched to the desired angles of attack (or yaw) and the surface pressures read on the manometers.

Pressure measurements were obtained for angles of attack of 0°, $\pm 2^{\circ}$, $\pm 4^{\circ}$, $\pm 6^{\circ}$, $+ 8^{\circ}$, $+ 10^{\circ}$, and $+ 14^{\circ}$; and for yaw angles of $\pm 2^{\circ}$, $\pm 4^{\circ}$, $\pm 6^{\circ}$, $\pm 8^{\circ}$, and $\pm 10^{\circ}$. Schlieren photographs were also taken at these angles of attack and yaw. The pressure measurements are

estimated to be accurate within $\pm$ 1 per cent, and the angles of attack and yaw accurate within $\pm$ 0.1 degrees.

B. Results and Discussion

Schlieren photographs are shown in Figures 4 through 15. By comparing Figures 4 and 10 for the model at zero angle of attack and zero yaw angle, one sees that the distance between the shock wave and the body is greater in the meridian plane containing the minor axis than in the meridian plane containing the major axis. Thus, the shock wave is not an ellipse similar to the body, but is "pushed in" toward the major axis and "pulled out" from the minor axis. This shape is to be expected from physical reasoning, since there is a cross flow from the high pressure sides at the ends of the major axis to the low pressure sides at the ends of the minor axis. This cross-flow tends to relieve the pressure somewhat at the high pressure sides and raise the pressure at the low pressure sides, thus causing a corresponding change in shock wave angle.

The surface pressure distributions are plotted in Figures 16 through 22, and the experimental pressure distributions are compared with the pressure distributions predicted by simple Newtonian theory in Figures 19, 20, and 21. For $\alpha = 0^{\circ}$, the Newtonian theory predicts surface pressures which are about fifty per cent too low on the low pressure sides of the cone (Figure 19), but are very close to the experimental values at the high pressure side. This result is expected from the physical argument given above, i. e., from the cross flow from high pressure to low pressure sides. As α increases, the Newtonian theory becomes

more and more accurate (Figure 10). This result is also expected, since at higher angles of attack the component of Mach number normal to the surface is larger, and the shock wave on the high pressure side is closer to the surface of the body.

In Figure 22 the experimental surface pressure distribution for $\alpha = 0^{\circ}$ is compared with the predictions of Newtonian theory, Van Dyke's second order slender body theory, and the present theory (Part II). The theory developed in Part II gives results which are closest to the experimental values, while the Newtonian theory predicts pressures which are too low over most of the surface, and the slender body theory also gives pressures which are too low.

IV. CONCLUSIONS AND SUMMARY

1. By applying approximations valid for hypersonic flow to Ferri's linearized characteristics method, simple algebraic expressions for the perturbation velocities are obtained for an unyawed conical body of arbitrary cross-section. Once these perturbation velocities are determined, the surface pressure distribution and the Fourier coefficients for the shock shape are readily calculated. The method is applied to an elliptic cone having a ratio of major to minor axis of 2:1, and a semi-vertex angle of about 12° in the meridian plane containing the major axis.

2. At zero yaw and pitch the experimentally-measured surface pressure distribution over the elliptic cone at $M = 5.8$ is predicted very closely by the present theory. On the other hand Van Dyke's second-order slender body theory and the simple Newtonian approximation both predict pressures that are too low.

3. Schlieren photographs of the shock surface taken at zero pitch and yaw in the planes containing the major and minor axes of the elliptic cross-section show that the shock surface lies considerably farther away from the body near the ends of the minor axis than it does near the ends of the major axis. This behavior is consistent with the "relieving effect" predicted on physical grounds, and helps to explain the calculated and measured surface pressure distribution.

4. As the angle of attack is increased the measured surface pressure distributions agree more and more closely with the Newtonian approximation. At the highest angle of attack ($\alpha = 14^{\circ}$) the Newtonian approximation is quite accurate.

5. Because of the encouraging results obtained for the unyawed elliptic cone, it seems worthwhile to investigate Ferri's suggestion that the flow over a yawed elliptic cone can be obtained by adding a contribution derived from the flow over a yawed circular cone, provided the angle of attack (or yaw) is not "too large".

REFERENCES

1. Van Dyke, M. D.: The Elliptic Cone as a Model for Non-Linear Supersonic Flow Theory. Journal of Fluid Mechanics, Vol. 1, Part 1, pp. 1-15.

2. Ferri, A.; Ness, N.; and Kaplita, T.: Supersonic Flow over Conical Bodies without Axial Symmetry. Journal of the Aeronautical Sciences, 20, 563-571, (1953).

3. Seaman, D., and Dore, F.: Force and Pressure Coefficients of Elliptic Cones and Cylinders in Newtonian Flow. Consolidated-Vultee Report ZA-7-004, (1952).

4. Fraenkel, L. E.: Supersonic Flow Past Slender Bodies of Elliptic Cross-Section. ARC, R and M 2954, (1955).

5. Jorgensen, L.: Elliptic Cones Alone and with Wings at Supersonic Speeds. NACA TN 4045, (1957).

6. Ferri, A.: The Linearized Characteristics Method and Its Application to Practical Nonlinear Supersonic Problems. NACA TN 2515, (1951).

7. Ness, N., and Kaplita, T.: Tabulated Values of Linearized Conical Flow Solutions for Solution of Supersonic Conical Flows without Axial Symmetry. PIBAL Report No. 220, (1954).

8. Lees, L.: Note on the Hypersonic Similarity Law for an Unyawed Cone. Journal of the Aeronautical Sciences, 18, 700-702, (1951).

9. Rogers, E. W. E., and Berry, C. J.: Experiments at M = 1.41 on Elliptic Cones with Subsonic Leading Edges. British ARC 17929, FM 2307, Perf. 1391, October 11, 1955.

10. Maslen, S.: Pressure Distribution on Thin Conical Body of Elliptic Cross Section at M = 1.89. NACA RM E8K05, (1949).

11. Eimer, M.: Direct Measurement of Laminar Skin Friction at Hypersonic Speeds. GALCIT Hypersonic Wind Tunnel Memorandum No. 16, July 1, 1953.

12. Vaglio-Laurin, R. and Van Dyke, M. D.: A Discussion of Higher-Order Approximations for the Flow Field about a Slender Elliptic Cone. Journal of Fluid Mechanics, Vol. 3, Part 6, March, 1958.

APPENDIX 1

HYPERSONIC APPROXIMATIONS FOR

$$\frac{\gamma-1}{2}\left(\frac{1-u_o^2}{u_o^2}\right)_{\theta_{oc}}\left(\frac{s'}{\gamma R}\right) \text{ AND } \left(\frac{u_o^2}{1-u_o^2}\right)_{\theta_{oc}}$$

The change in entropy across a shock wave of angle θ_s is given by the following expression:

$$e^{-(\Delta s)/R} = \left[\frac{(\gamma+1)\,M_1^2\sin^2\theta_s}{(\gamma-1)\,M_1^2\sin^2\theta_s+2}\right]^{\frac{\gamma}{\gamma-1}}\left[\frac{\gamma+1}{2\gamma M_1^2\sin^2\theta_s-(\gamma-1)}\right]^{\frac{1}{\gamma-1}}$$

Therefore, for constant γ and R

$$\frac{s'}{\gamma R} = \left[\frac{d}{d\theta_s}\left(\frac{\Delta s}{\gamma R}\right)\right]_{\theta_{os}} = 4\cot\theta_{os}\,\frac{(M_1^2\sin^2\theta_{os}-1)^2}{\left[2\gamma M_1^2\sin^2\theta_{os}-(\gamma-1)\right]\left[(\gamma-1)M_1^2\sin^2\theta_{os}+2\right]}$$

$$\cong \frac{4}{\theta_{os}}\,\frac{(K_s^2-1)^2}{\left[2\gamma K_s^2-(\gamma-1)\right]\left[(\gamma-1)K_s^2+2\right]}$$

where $K_s = M_1\,\theta_{os}$. From Equation (5) of Reference 8, it is easily seen that

$$\frac{\gamma-1}{2}\left(\frac{1-u_o^2}{u_o^2}\right)_{\theta_{oc}} \cong \frac{(\gamma-1)K_s^2+2}{2M_1^2}$$

Therefore,

$$\frac{\gamma-1}{2}\left(\frac{1-u_o^2}{u_o^2}\right)_{\theta_{oc}}\left(\frac{s'}{\gamma R}\right) \cong \frac{2}{M_1 K_s}\left[\frac{(K_s^2-1)^2}{2\gamma K_s^2-(\gamma-1)}\right]$$

To obtain an expression for $\left(\frac{u_o^2}{1 - u_o^2} \right)_{\theta_{oc}}$ in terms of $(\theta - \theta_{oc})$, use is made of the fact that at $\theta = \theta_{os}$,

$$- \frac{\gamma - 1}{\gamma + 1} \left(\frac{1 - u_o^2}{u_o v_o} \right)_{\theta_{os}} = \tan \theta_{os} \quad *$$

From Equation (39) it is seen that

$$\left(\frac{u_o^2}{1 - u_o^2} \right)_{\theta_{os}} = \frac{\gamma - 1}{\gamma + 1} \left(\frac{u_o}{v_o} \right)_{\theta_{os}} \cot \theta_{os} \cong \frac{1}{2} \frac{\gamma - 1}{\gamma + 1} \frac{\cot \theta_{os}}{\theta_{os} - \theta_{oc}}$$

But

$$\left(\frac{u_o^2}{1 - u_o^2} \right)_{\theta_{os}} \cong \left(\frac{u_o^2}{1 - u_o^2} \right)_{\theta_{oc}}$$

Therefore,

$$\left(\frac{u_o^2}{1 - u_o^2} \right)_{\theta_{oc}} \cong \frac{1}{2} \frac{\gamma - 1}{\gamma + 1} \frac{\cot \theta_{os}}{\theta_{os} - \theta_{oc}}$$

---

* This relation is easily derived from Equations (15) and (16).

APPENDIX 2

CORRECTION FOR FIRST APPROXIMATION FOR u_n AND v_n

If the expression for $\partial u_n/\partial\theta$ from Equation (44) is substituted into the first term on the right hand side of Equation (43), this term takes the following form:

$$\frac{4}{\gamma+1}\left(\frac{\theta-\theta_{oc}}{\theta_{os}-\theta_{oc}}\right)\frac{1}{\theta_{os}}\frac{\partial u_n}{\partial\theta} \cong \frac{8}{\gamma-1}\left(\frac{u_o^2}{1-u_o^2}\right)_{\theta_{oc}}(\theta-\theta_{oc})\frac{\partial u_n}{\partial\theta}$$

$$= \frac{8}{\gamma-1}\left(\frac{u_o^2}{1-u_o^2}\right)_{\theta_{oc}} n\left(\frac{\theta-\theta_{oc}}{\theta}\right)(A\theta^n - B\theta^{-n})$$

The method of variation of parameters is now used to obtain a particular solution which is a correction to the first approximation for u_n and v_n. The corrected expressions for u_n and v_n are given by the expressions

$$u_n = C\theta^n + D\theta^{-n} + \int_{\theta_{oc}}^{\theta}\left[\left(\frac{\theta}{t}\right)^n - \left(\frac{t}{\theta}\right)^n \frac{t}{2n}\right] s(t)\,dt \quad ,$$

and

$$v_n = \frac{n}{\theta}\left\{C\theta^n - D\theta^{-n} + \int_{\theta_{oc}}^{\theta}\left[\left(\frac{\theta}{t}\right)^n + \left(\frac{t}{\theta}\right)^n\right]\frac{t}{2n}\, s(t)\,dt\right\} \quad ,$$

where

$$\frac{t}{2n}\,s(t) = \frac{4}{\gamma-1}\left(\frac{u_o^2}{1-u_o^2}\right)_{\theta_{oc}}(t-\theta_{oc})(At^n - Bt^{-n})$$

and A and B are given in Equation (44).

The values of C and D obtained by utilizing the boundary conditions on u_n, v_n, and w_n at $\theta = \theta_{os}$ are as follows:

$$C = A\left\{1 - \frac{2}{\gamma-1}\left(\frac{u_o^2}{1-u_o^2}\right)_{\theta_{oc}} \int_{\theta_{oc}}^{\theta_{os}} \left[\left(1+\frac{\theta_{os}}{n}\right) - \left(1-\frac{\theta_{os}}{n}\right)\left(\frac{t}{\theta_{os}}\right)^{2n}\right](t-\theta_{oc})\,dt\right\}$$

$$- \frac{2}{\gamma-1}\left(\frac{u_o^2}{1-u_o^2}\right)_{\theta_{oc}} B\theta_{os}^{-2n} \int_{\theta_{oc}}^{\theta_{os}} \left[\left(1-\frac{\theta_{os}}{n}\right) - \left(1+\frac{\theta_{os}}{n}\right)\left(\frac{\theta_{os}}{t}\right)^{2n}\right](t-\theta_{oc})\,dt$$

$$D = B\left\{1 - \frac{2}{\gamma-1}\left(\frac{u_o^2}{1-u_o^2}\right)_{\theta_{oc}} \int_{\theta_{oc}}^{\theta_{os}} \left[\left(1+\frac{\theta_{os}}{n}\right) - \left(1-\frac{\theta_{os}}{n}\right)\left(\frac{\theta_{os}}{t}\right)^{2n}\right](t-\theta_{oc})\,dt\right\}$$

$$- \frac{2}{\gamma-1}\left(\frac{u_o^2}{1-u_o^2}\right)_{\theta_{oc}} A\,\theta_{os}^{2n} \int_{\theta_{oc}}^{\theta_{os}} \left[\left(1-\frac{\theta_{os}}{n}\right) - \left(1+\frac{\theta_{os}}{n}\right)\left(\frac{t}{\theta_{os}}\right)^{2n}\right](t-\theta_{oc})\,dt$$

By evaluating the integrals in these ~~procedures~~ EXPRESSIONS the following relations are finally obtained for C and D:

$$C = A\left\{1 - \frac{1}{\gamma-1}\left(\frac{u_o^2}{1-u_o^2}\right)_{\theta_{oc}} (\theta_{os}-\theta_{oc})^2 \left[1 + \frac{\theta_{os}}{n} + \left(\frac{\theta_{oc}}{\theta_{os}}\right)^{2n} \frac{1-\frac{\theta_{os}}{n}}{(2n+1)(n+1)}\right]\right\}$$

$$- B\,\theta_{os}^{-2n} \frac{1}{\gamma-1}\left(\frac{u_o^2}{1-u_o^2}\right)_{\theta_{oc}} (\theta_{os}-\theta_{oc})^2 \left[1 - \frac{\theta_{os}}{n} + \left(\frac{\theta_{oc}}{\theta_{os}}\right)^{2n} \frac{1+\frac{\theta_{os}}{n}}{(2n-1)(n-1)}\right]$$

$$D = B\left\{1 - \frac{1}{\gamma-1}\left(\frac{u_o^2}{1-u_o^2}\right)\theta_{oc}(\theta_{os}-\theta_{oc})^2\left[1+\frac{\theta_{os}}{n}+\left(\frac{\theta_{os}}{\theta_{oc}}\right)^{2n}\frac{1-\frac{\theta_{os}}{n}}{(2n-1)(n-1)}\right]\right\}$$

$$- A\,\theta_{os}^{2n}\,\frac{1}{\gamma-1}\left(\frac{u_o^2}{1-u_o^2}\right)\theta_{oc}(\theta_{os}-\theta_{oc})^2\left[1-\frac{\theta_{os}}{n}+\left(\frac{\theta_{oc}}{\theta_{os}}\right)^{2n}\frac{1+\frac{\theta_{os}}{n}}{(2n+1)(n+1)}\right]$$

$$n \neq 1$$

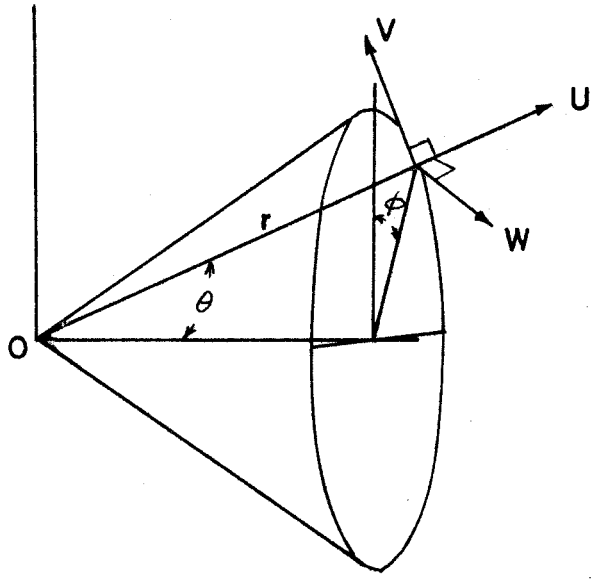

FIG. 1 COORDINATE SYSTEM AND VELOCITY COMPONENTS

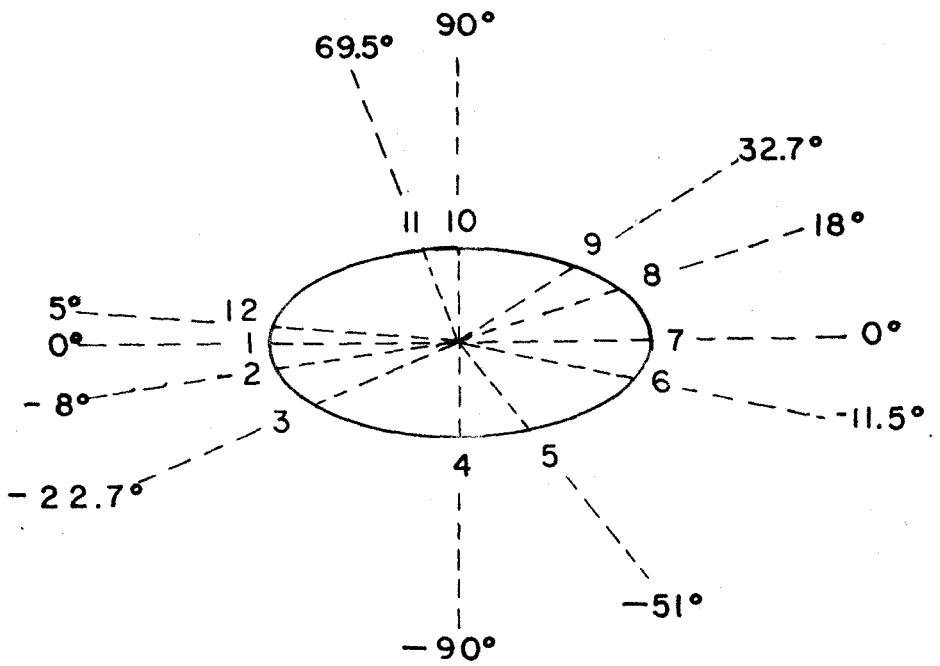

Angle of Attack

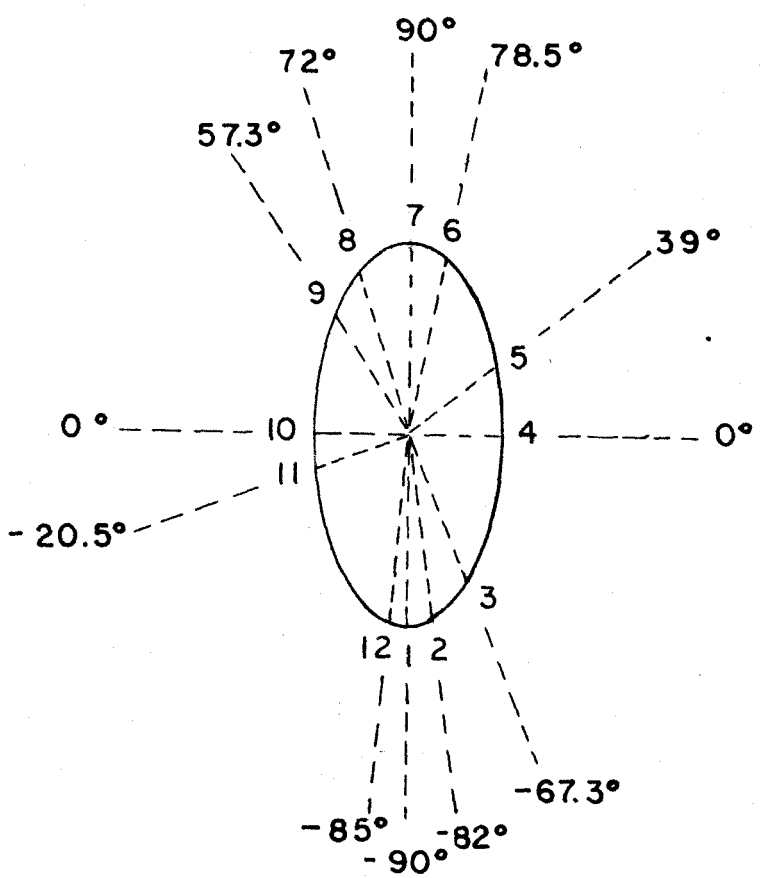

Yaw

FIG. 2 ORIFICE LOCATION AND NOTATION

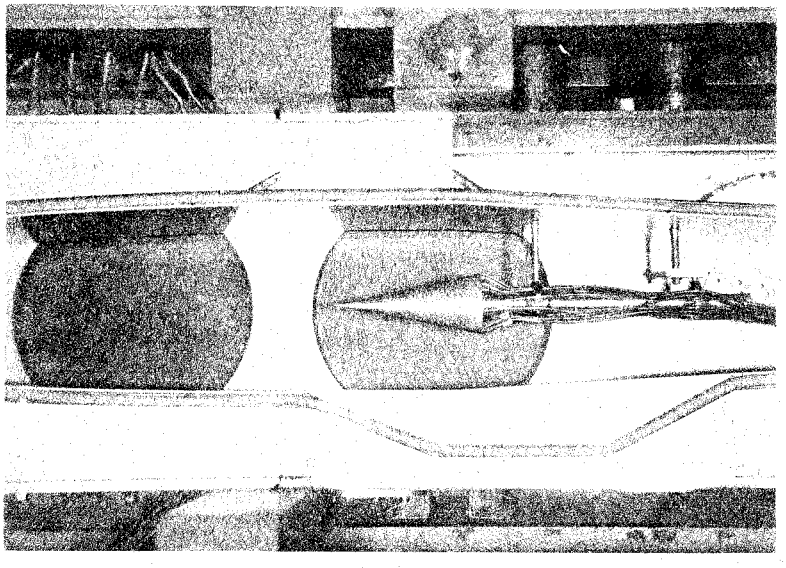

FIG. 3

TUNNEL SETUP

FIG. 4

SCHLIEREN PHOTOGRAPH AT $\alpha = 0^{o}$

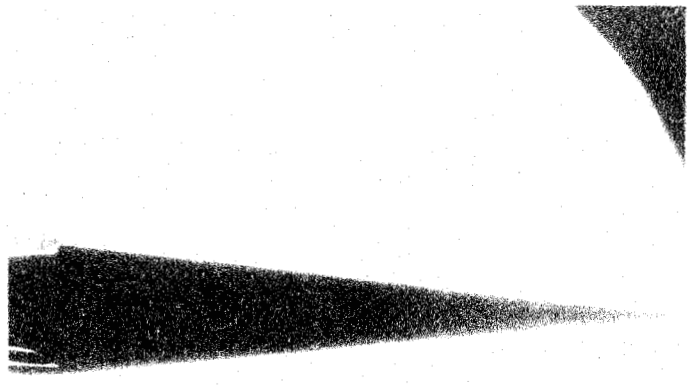

FIG. 5

SCHLIEREN PHOTOGRAPH AT $\alpha = 2^{o}$

FIG. 6

SCHLIEREN PHOTOGRAPH AT $\alpha = 4^{o}$

FIG. 7

SCHLIEREN PHOTOGRAPH AT $\alpha = 8^{o}$

FIG. 8

SCHLIEREN PHOTOGRAPH AT $\alpha = 10^{\circ}$

FIG. 9

SCHLIEREN PHOTOGRAPH AT $\alpha = 14^{\circ}$

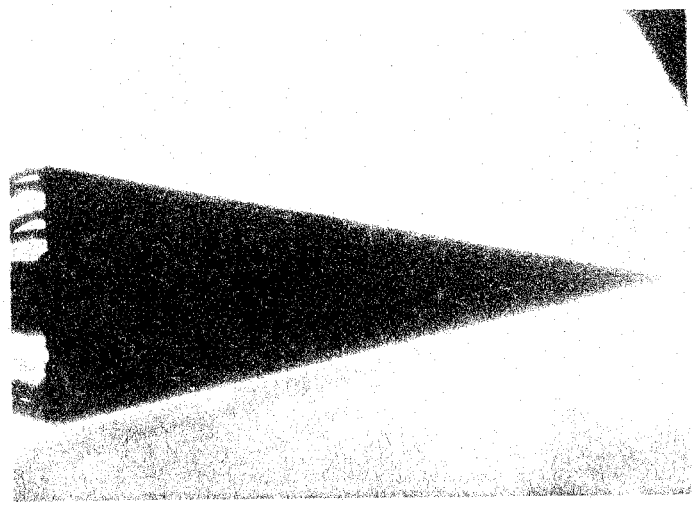

FIG. 10

SCHLIEREN PHOTOGRAPH AT $\psi = 0^{\circ}$

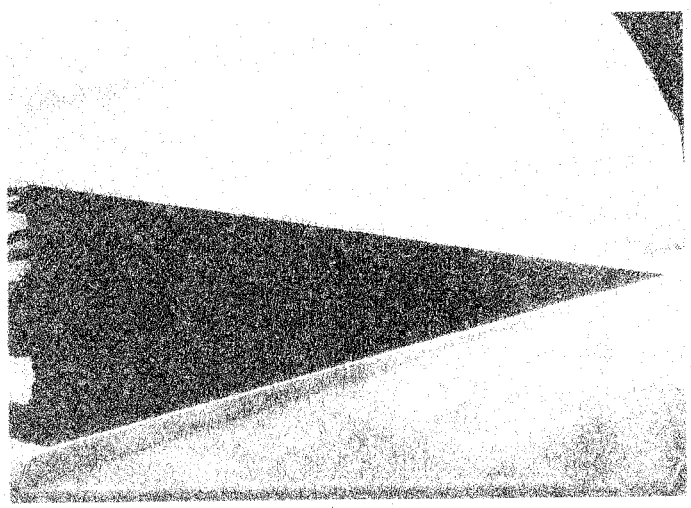

FIG. 11

SCHLIEREN PHOTOGRAPH AT $\psi = 2^{\circ}$

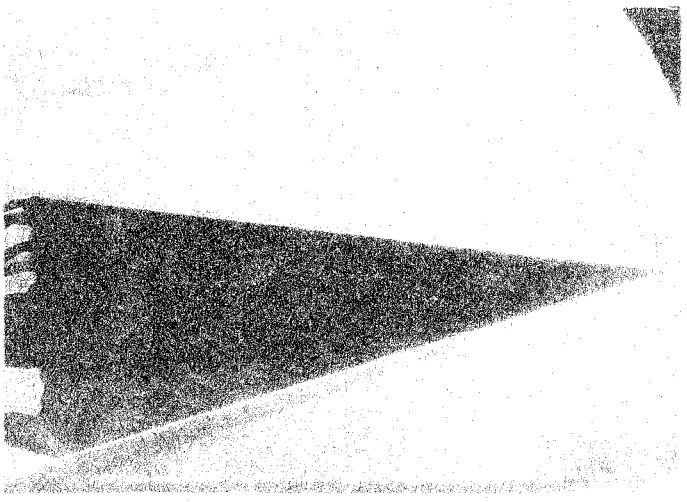

FIG. 12

SCHLIEREN PHOTOGRAPH AT $\psi = 4^{\circ}$

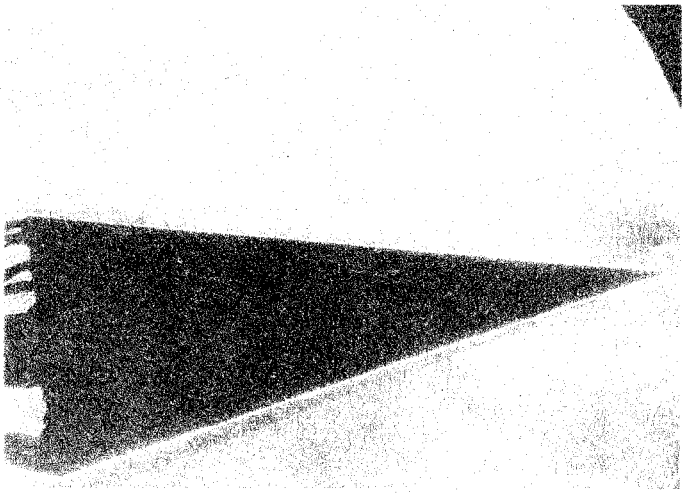

FIG. 13

SCHLIEREN PHOTOGRAPH AT $\psi = 6^{\circ}$

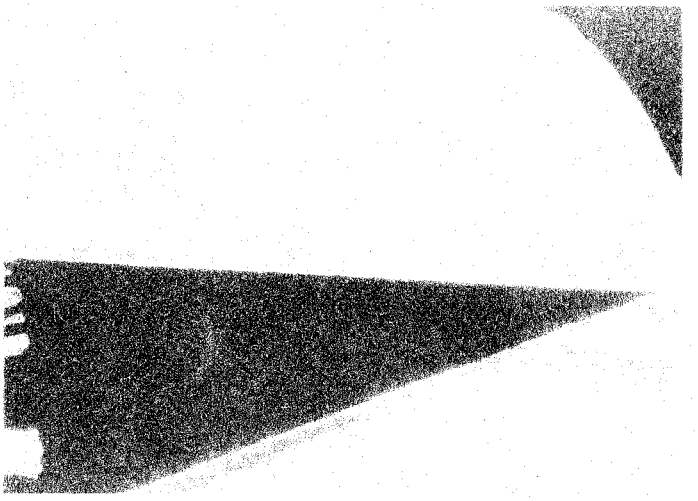

FIG. 14

SCHLIEREN PHOTOGRAPH AT $\psi = 8^{\circ}$

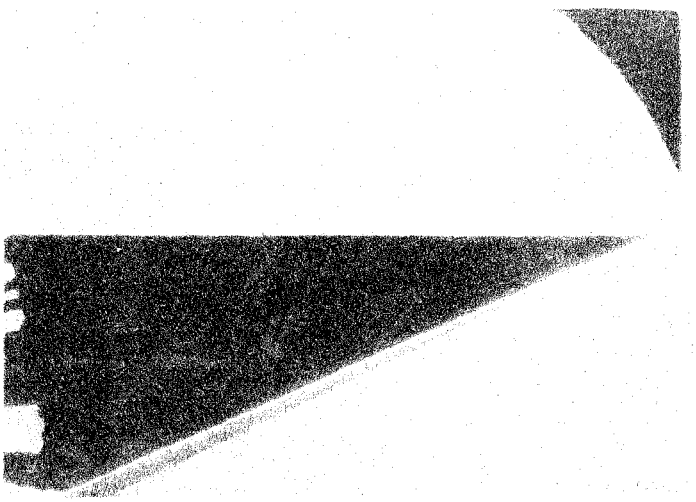

FIG. 15

SCHLIEREN PHOTOGRAPH AT $\psi = 10^{\circ}$

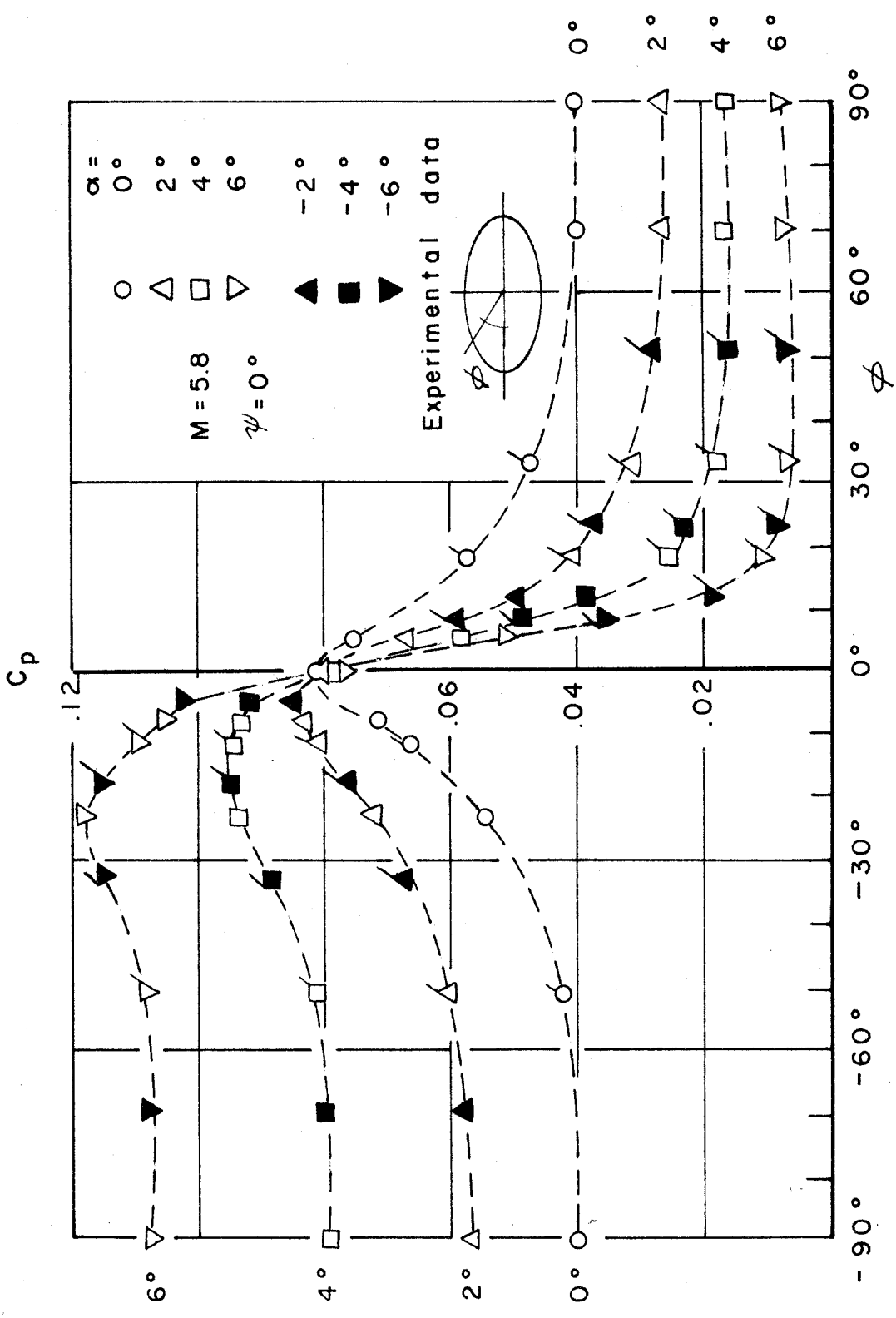

FIG. 16 SURFACE PRESSURE DISTRIBUTION, $\alpha = 0°, 2°, 4°, 6°$

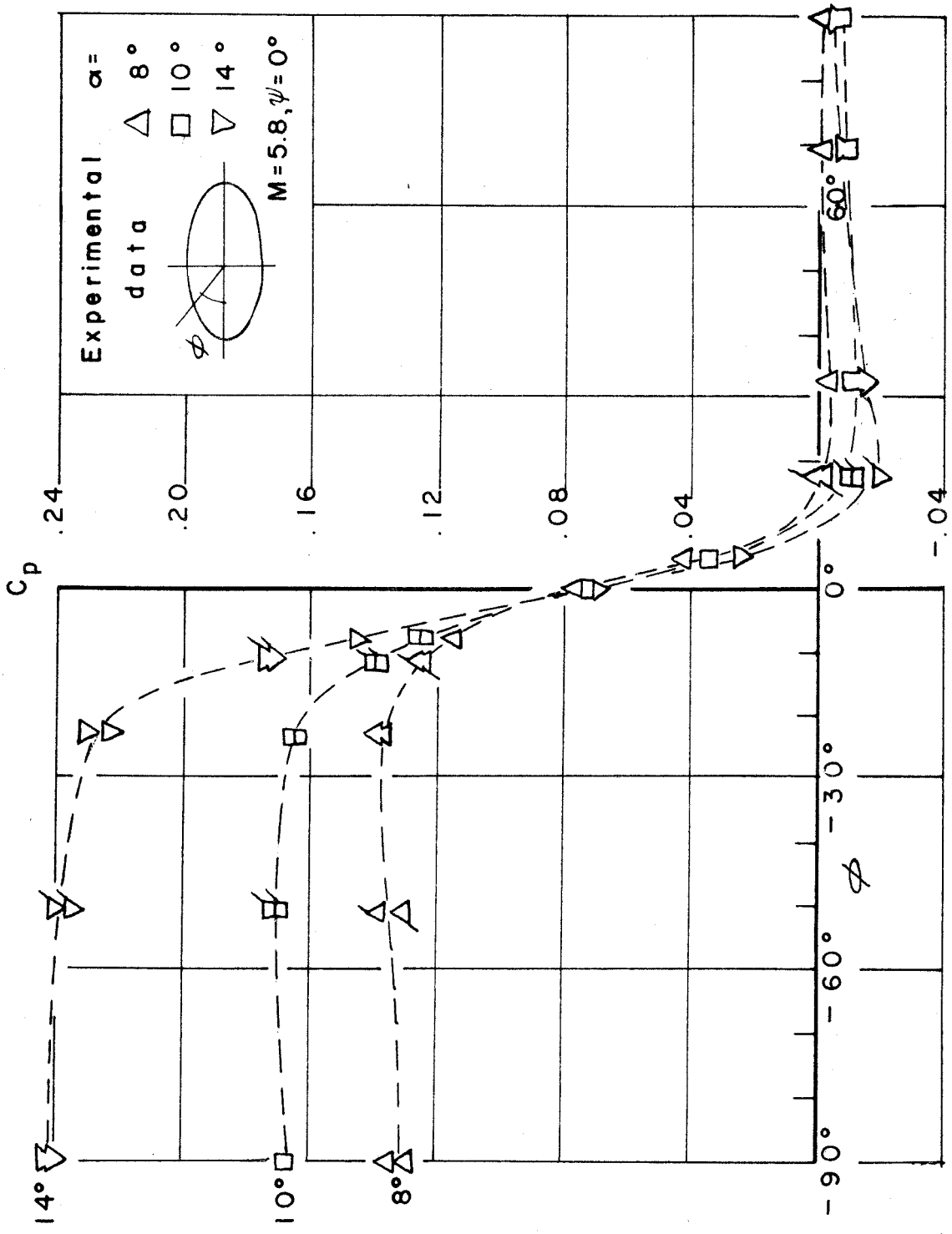

FIG.17 SURFACE PRESSURE DISTRIBUTION, α= 8°,10°,14°

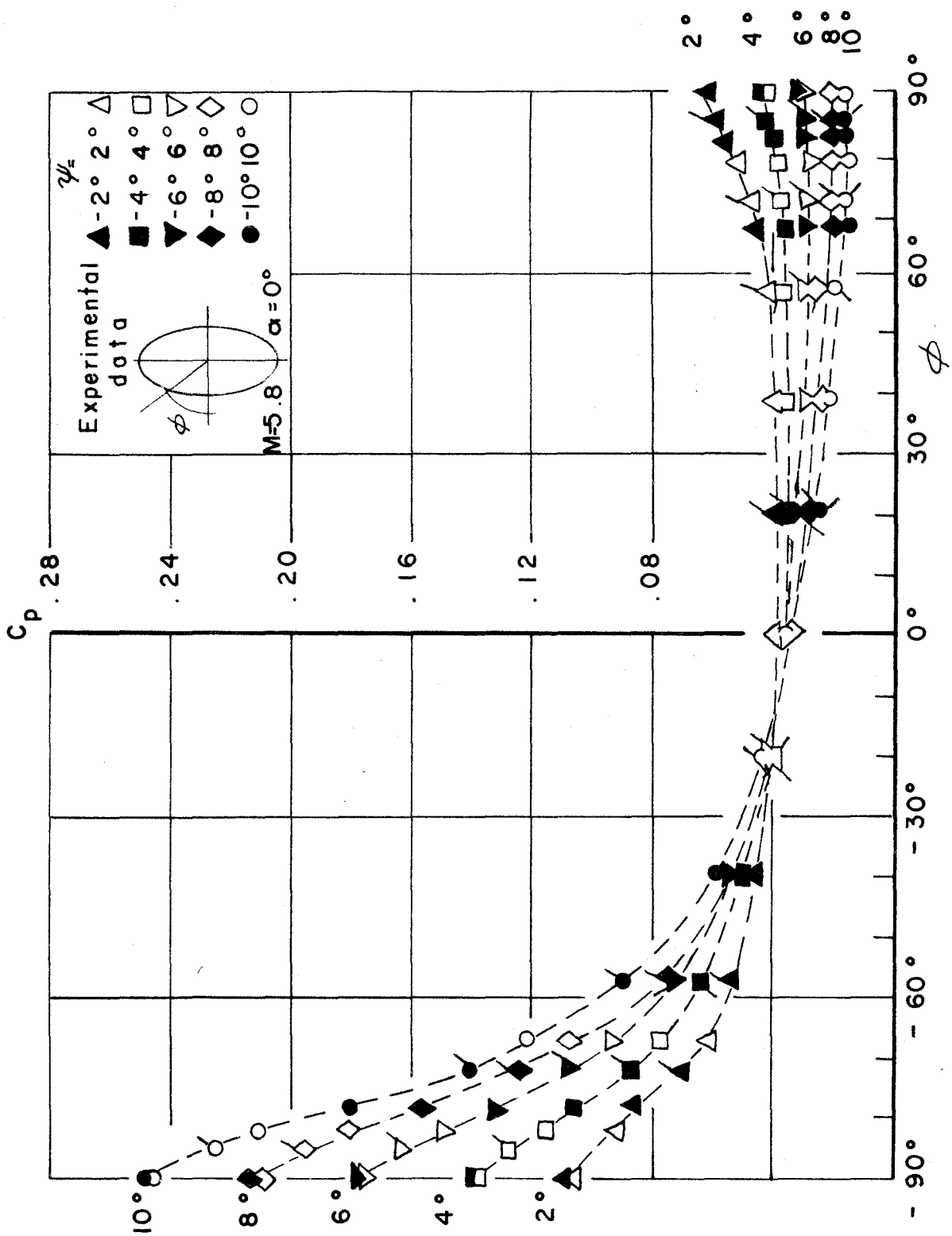

FIG.18 SURFACE PRESSURE DISTRIBUTION, ψ = 2°, 4°, 6°, 8°, 10°

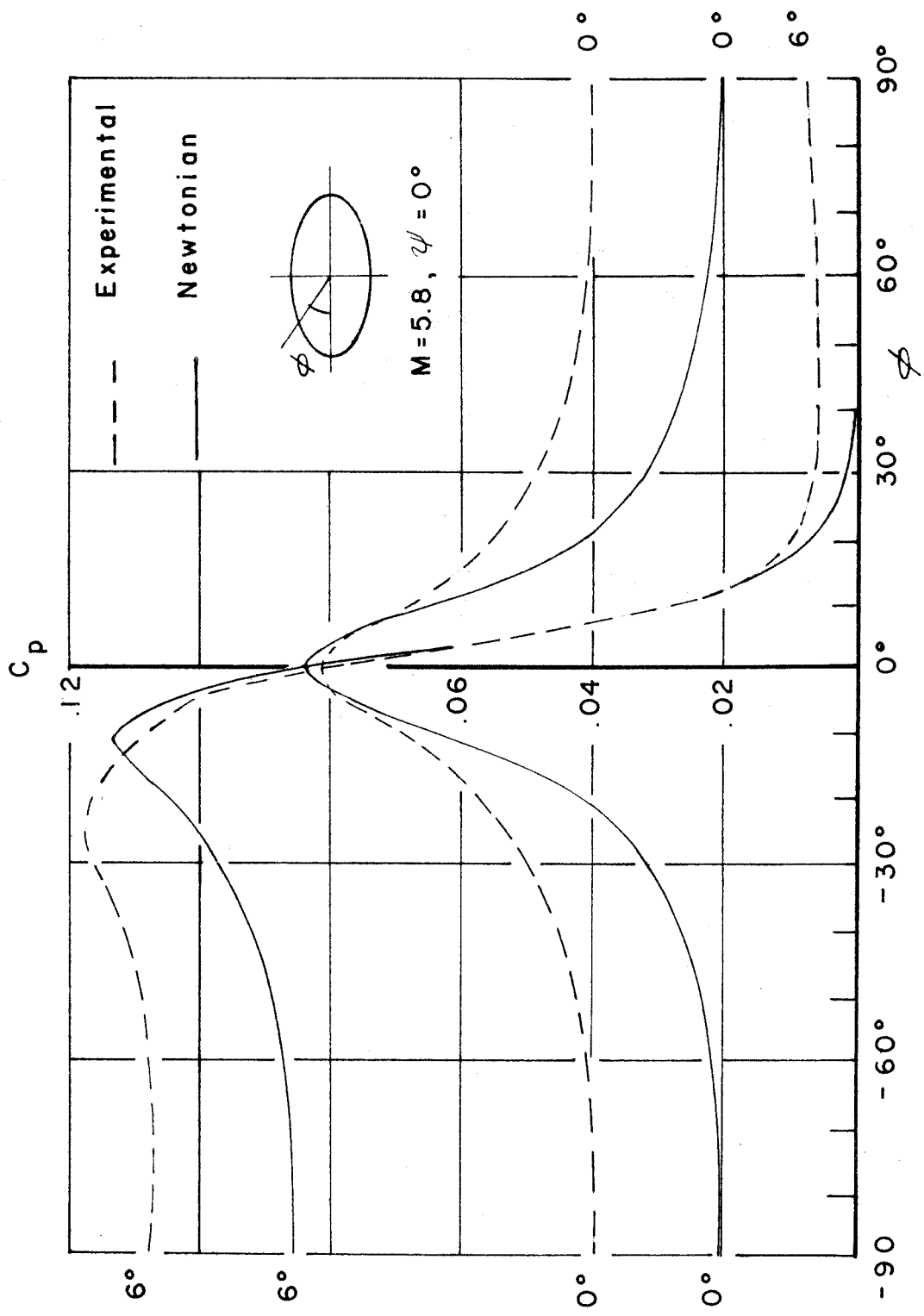

FIG.19 SURFACE PRESSURE DISTRIBUTION, α = 0°, 6°

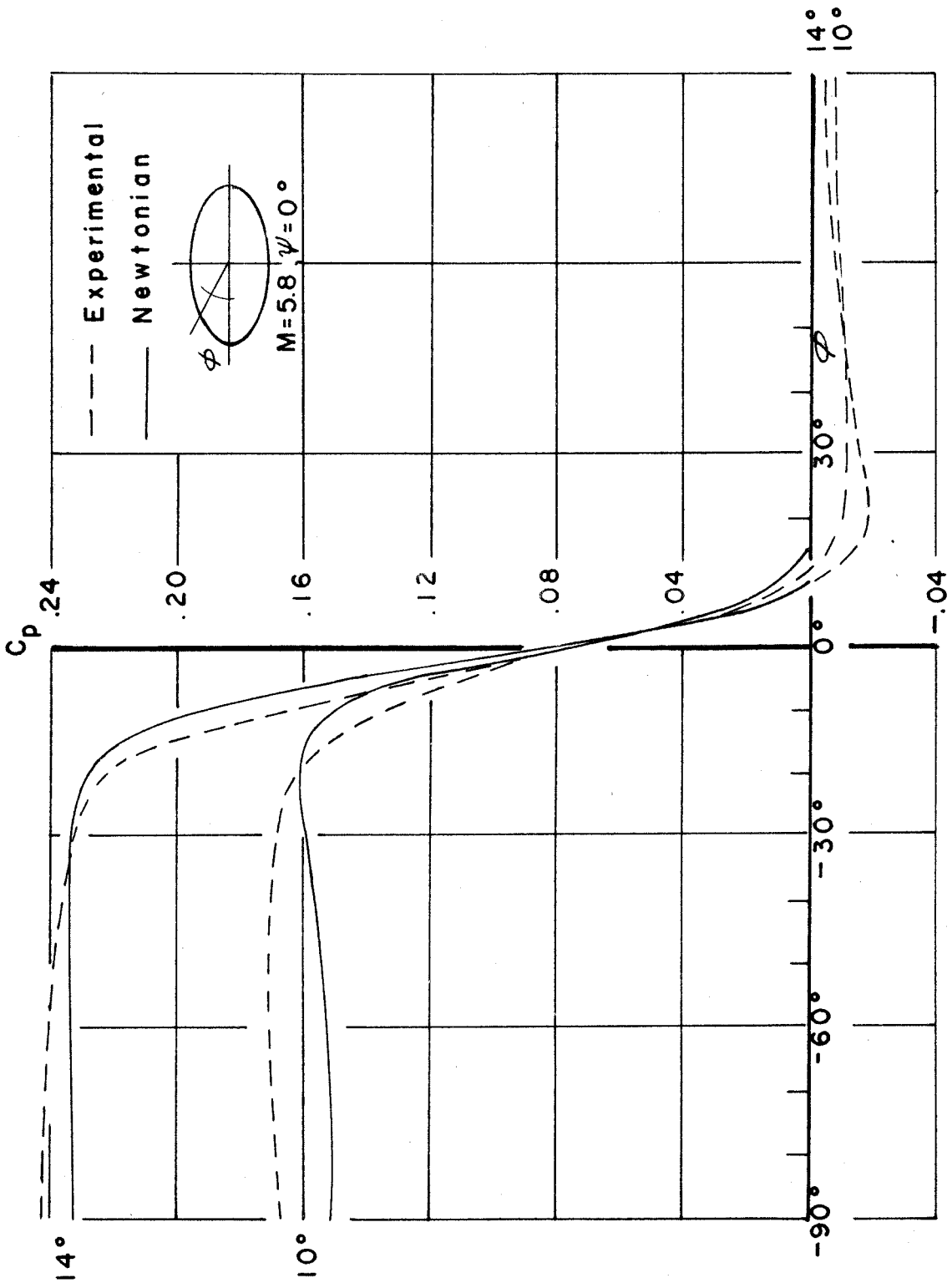

FIG. 20 SURFACE PRESSURE DISTRIBUTION, $\alpha = 10°, 14°$

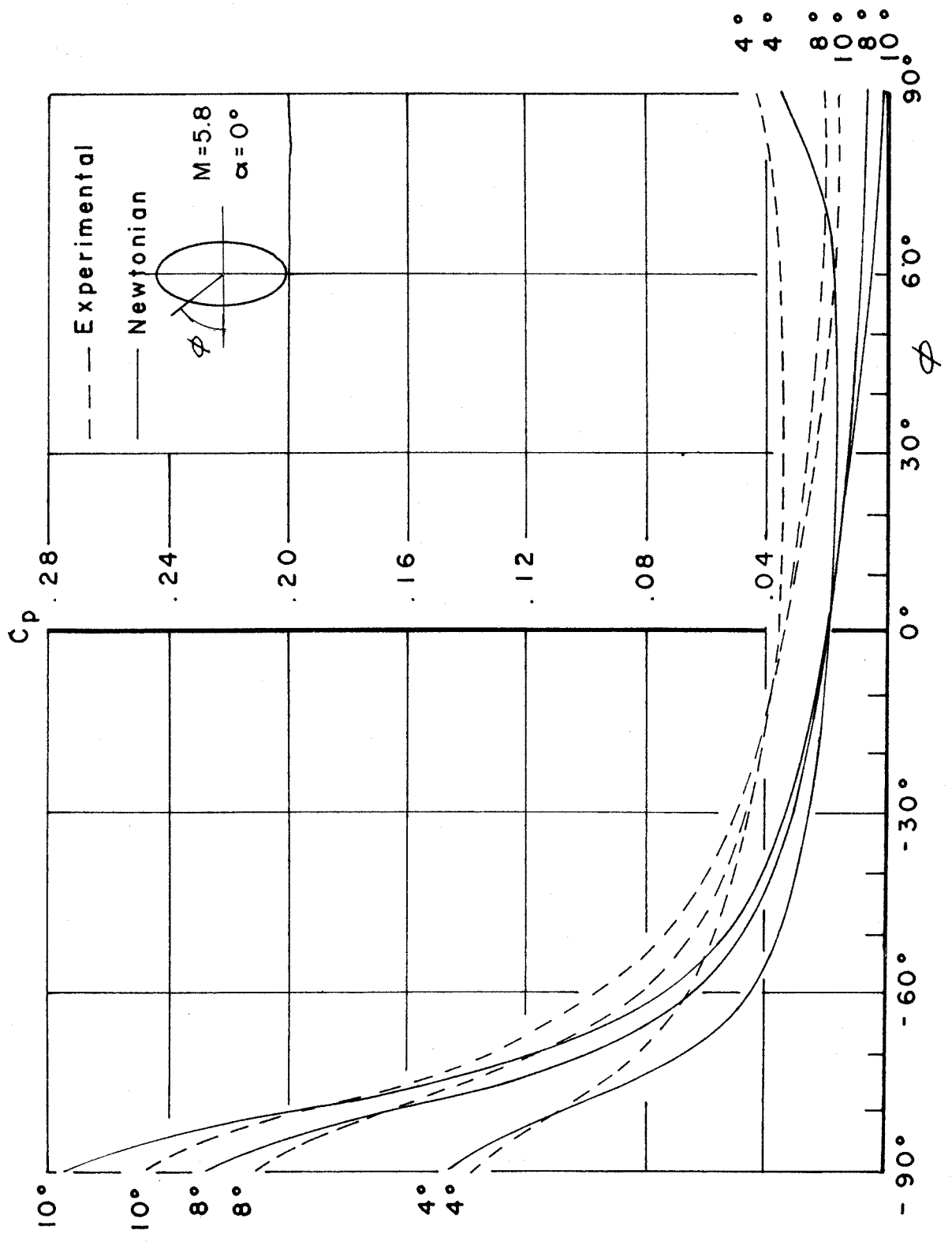

FIG.21 SURFACE PRESSURE DISTRIBUTION, ψ= 4°, 8°, 10°

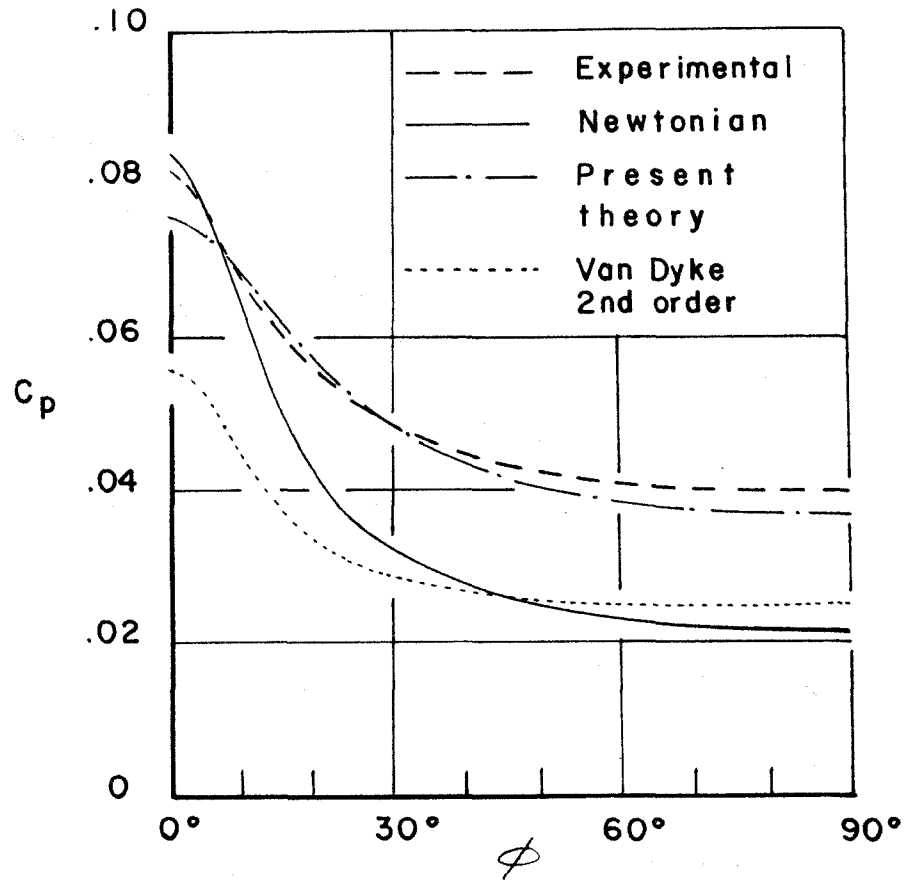

FIG. 22 SURFACE PRESSURE DISTRIBUTION, $\alpha = 0°$